Received: 13 July 2020 | Accepted: 10 November 2020

DOI: 10.1002/pamm.202000175

# 3D Virtual Elements for Elastodynamic Problems

**Mertcan Cihan**[1,*], **Fadi Aldakheel**[1,**], **Blaž Hudobivnik**[1,***], and **Peter Wriggers**[1,†]

[1] Leibniz Universität Hannover (LUH), Institute of Continuum Mechanics (IKM), An der Universität 1, 30823 Garbsen, Germany

A virtual element framework for nonlinear elastodynamics is outlined within this work. The virtual element method (VEM) can be considered as an extension of the classical finite element method. While the finite element method (FEM) is restricted to the usage of regular shaped elements, VEM allows to use non-convex shaped elements for the spatial discretization [1]. It has been applied to various engineering problems in elasticity and other areas, such as plasticity or fracture mechanics as outlined in [3, 4]. This work deals with the extension of VEM to dynamic problems. Low-order ansatz functions in two and three dimensions, with elements being arbitrary shaped, are used in this contribution. The formulations considered in this framework are based on minimization of energy, where a pseudo potential is used for the dynamic behavior. While the stiffness-matrix needs a suitable stabilization, the mass-matrix can be calculated fully through the projection part. For the implicit time integration, Newmark-Method is used. To show the performance of the method, various numerical examples in 2D and 3D are presented.



## 1 Introduction

The possibility of using arbitrary shaped elements gives more flexibility and new possibilities to geometry discretization in solid- and fluid-mechanics. Due to this fact, VEM increases the variety of possible applications in engineering and science. Up to now, VEM has been investigated, inter alia, for elasto-plastic deformations, considering thermal effects, in [4], hyperelastic materials at finite deformations in [7], crack-propagation for 2D elastic solids at small strains in [3] and phase-field modeling of brittle and ductile fracture in [2, 6].
Despite the fact that dynamic behavior has a strong influence on the mechanical properties and the prediction of their real response, the investigations introduced above are only done for static problems so far. This has motivated the authors in [5] to extend the application of VEM from the static to the dynamic case in the finite deformation range.

## 2 Formulation of the virtual element method

### 2.1 The VEM Ansatz

The main idea of the virtual element method relies on the split of the ansatz space $\boldsymbol{u}_h$ into a projected part $\boldsymbol{u}_\Pi$ and a remainder $\boldsymbol{u}_h - \boldsymbol{u}_\Pi$ as

$$\boldsymbol{u}_h = \boldsymbol{u}_\Pi + (\boldsymbol{u}_h - \boldsymbol{u}_\Pi) \tag{1}$$

For a low order linear ansatz, the projection $\boldsymbol{u}_\Pi$ at element level takes for three-dimensional elements the form

$$\boldsymbol{u}_\Pi = \mathbf{H}\,\mathbf{a} \qquad \text{with} \qquad \mathbf{H} = \begin{bmatrix} 1 & 0 & 0 & X & 0 & 0 & Y & 0 & 0 & Z & 0 & 0 \\ 0 & 1 & 0 & 0 & X & 0 & 0 & Y & 0 & 0 & Z & 0 \\ 0 & 0 & 1 & 0 & 0 & X & 0 & 0 & Y & 0 & 0 & Z \end{bmatrix} , \tag{2}$$

where $\mathbf{a}$ represents the twelve unknown virtual parameter $\mathbf{a} = \bigcup \mathbf{a}_i$ which have to be determined. The unknown virtual parameters can be computed implicitly with the help of the following condition, see [7]:

$$\nabla \boldsymbol{u}_\Pi \overset{!}{=} \frac{1}{\Omega_e} \int_{\Gamma_e} \boldsymbol{u}_h \otimes \boldsymbol{N} \; d\Gamma \, , \tag{3}$$

where $\boldsymbol{N}$ denotes the outward normal vector on the reference boundary $\Gamma_e$ of the domain $\Omega_e$, which belongs to a virtual element $e$. Since the space of employed ansatz functions is linear, the gradient of the projected displacements (left hand side

* Corresponding author: e-mail Cihan@ikm.uni-hannover.de, phone +49 511 762 17560, fax +49 511 762 5496
** e-mail Aldakheel@ikm.uni-hannover.de
*** e-mail Hudobivnik@ikm.uni-hannover.de
† e-mail Wriggers@ikm.uni-hannover.de

of (3)) are constant over the entire element and takes the simple form:

$$\nabla \boldsymbol{u}_{\Pi} = \begin{bmatrix} a_{1\,2} & a_{1\,3} & a_{1\,4} \\ a_{2\,2} & a_{2\,3} & a_{2\,4} \\ a_{3\,2} & a_{3\,3} & a_{3\,4} \end{bmatrix} \tag{4}$$

For 2D elements, the right hand side of equation (3) can simply be evaluated at the edges of the element, which are line segments. Using linear ansatz, the displacements at the boundary of the element are known at the straight line segments, see [7]. Simply speaking, the virtual parameters in (4) are linked to the known nodal displacements at the boundary of the virtual element. For the 3D case, the computation of the virtual parameters is not straight forward. Here, the boundary of the element consists of 2D polygonal faces. Therefore an appropriate way is to sub triangulate the polygon in to three noded triangles and use standard ansatz function for a linear triangle with the associated Gauss points, as described in [7]. Up to now, we are only able to compute the virtual parameters which are related to the gradient of the projected displacement (4). Further we need to compute the three unknown virtual parameters $\mathbf{a}_{i1}, i \subset 1,2,3$, which are related to a constant strain field. To ensure uniqueness, we adopt the condition, that the sum of the nodal values of $\boldsymbol{u}_h$ and of its projection $\boldsymbol{u}_{\Pi}$ are equal, see [5,7]:

$$\frac{1}{n_V}\sum_{I=1}^{n_V} \boldsymbol{u}_{\Pi}(\mathbf{X}_I) = \frac{1}{n_V}\sum_{I=1}^{n_V} \boldsymbol{u}_h(\mathbf{X}_I)\,, \tag{5}$$

where $\mathbf{X}_I$ are the coordinates of the nodal point $I$.

### 2.2 Construction of the element mass-matrix for vem

For the computation of the element mass-matrix the same split is used for the accelerations $\ddot{\boldsymbol{u}}_h$ as for the displacements in (1):

$$\ddot{\boldsymbol{u}}_h = \ddot{\boldsymbol{u}}_{\Pi} + (\ddot{\boldsymbol{u}}_h - \ddot{\boldsymbol{u}}_{\Pi})\,, \tag{6}$$

where $\ddot{\boldsymbol{u}}_{\Pi}$ are the projected accelerations. For the computation of the projected accelerations, we use the same ansatz and same conditions (3) and (5) as for the projected displacements:

$$\ddot{\boldsymbol{u}}_{\Pi} = \mathbf{H}\,\ddot{\mathbf{a}}\,, \tag{7}$$

where $\ddot{\mathbf{a}}$ denote the virtual accelerations. To construct an elastodynamic virtual element, it is computationally advantageous to use the software tool *AceGen*, see [7]. The construction of the element mass-matrix starts from the pseudo-potential:

$$U^{dyn}(\boldsymbol{u}) = \int_{\Omega} \rho\ddot{\boldsymbol{u}} \cdot \boldsymbol{u}\, d\Omega\,, \tag{8}$$

Using the Implicit Newmark method for the implicit time integration and taking the first variation while holding the acceleration $\ddot{\boldsymbol{u}}$ constant, the residual takes the form:

$$\boldsymbol{R}^{dyn} = \left.\frac{\partial U^{dyn}(\boldsymbol{u}_{\Pi})}{\partial \boldsymbol{u}_e}\right|_{\ddot{\boldsymbol{u}}_e = const.} = \mathbf{M}\cdot\left[\frac{1}{\zeta\Delta t^2}(\boldsymbol{u}_{e,n+1} - \boldsymbol{u}_{e,n}) - \frac{1}{\zeta\Delta t}\dot{\boldsymbol{u}}_{e,n} - (\frac{1}{2\zeta} - 1)\ddot{\boldsymbol{u}}_{e,n}\right] \tag{9}$$

with the Newmark parameter $\zeta = 1/4$. The second derivative of (9) yields then to the dynamic part of the tangent:

$$\frac{\partial^2 U^{dyn}(\boldsymbol{u}_{\Pi}|_e)}{\partial \boldsymbol{u}_e^2} = \mathbf{M}\cdot\frac{1}{\zeta\Delta t^2} \quad \text{with} \quad \mathbf{M} = \left(\tilde{\mathbf{\Pi}}^{\nabla}\right)^T \int_{\Omega} \rho\mathbf{H}^T\mathbf{H}\, d\Omega\, \tilde{\mathbf{\Pi}}^{\nabla} \tag{10}$$

Here, $\mathbf{M}$ denotes the mass-matrix, which is fully computed through the projection part. The constant matrix $\tilde{\mathbf{\Pi}}^{\nabla}$ represents the projection operator and defined in [5].

### 2.3 Construction of the Virtual Element

As already mentioned, the formulation of an elastodynamic virtual element is based on a split of the energy in to a projected part $U_c(\boldsymbol{u}_{\Pi}|_e)$ and a stabilization part $U_{stab}(\boldsymbol{u}_h|_e - \boldsymbol{u}_{\Pi}|_e)$. The approximation of the projection part yields to a rank deficiency in the tangent and therefore needs to be stabilized. After summing up all element contributions for $\boldsymbol{n}_e$ elements, the total potential takes the form:

$$U(\boldsymbol{u}) = \mathop{\mathsf{A}}_{e=1}^{n_e} \left[U_c(\boldsymbol{u}_{\Pi}|_e) + U_{stab}(\boldsymbol{u}_h|_e - \boldsymbol{u}_{\Pi}|_e)\right] \tag{11}$$

 

where the projection part has the form:

$$U_c(\boldsymbol{u}_\Pi|_e) = \int_{\Omega_e} \left[\Psi(\boldsymbol{u}_\Pi) - \bar{\boldsymbol{f}} \cdot \boldsymbol{u}_\Pi\right] d\Omega - \int_{\Gamma_e^N} \bar{\boldsymbol{t}} \cdot \boldsymbol{u}_\Pi \, d\Gamma + \int_{\Omega_e} \rho \ddot{\boldsymbol{u}}_\Pi \cdot \boldsymbol{u}_\Pi \, d\Omega \tag{12}$$

Here, $\Psi(\boldsymbol{u}_\Pi)$ is the Neo-Hookean strain energy function, $\bar{\boldsymbol{t}}$ the surface tractions and $\bar{\boldsymbol{f}}$ the body forces. The projection part can be simply evaluated at the element centroid, see [5, 7]. The evaluation of the stabilization part can be realized through different methods. In this contribution, the stabilization part is computed on a submesh of 3 nodes triangles in 2D and 4 nodes tetrahedrons in 3D with linear shape functions, using the classical finite element method. For further details see [5, 7]. The final form of the tangent yields:

$$\mathbf{K_e} = (1-\beta^{stat})\mathbf{K_{c,e}}^{stat} + (1-\beta^{dyn})\mathbf{K_{c,e}}^{dyn} + \beta^{stat}\mathbf{K_{stab,e}}^{stat} + \beta^{dyn}\mathbf{K_{stab,e}}^{dyn}\,, \tag{13}$$

where $\beta^{stat}$ and $\beta^{dyn}$ are fraction parameters for the static and dynamic part. For $\beta = 1$ the tangent is obtained fully using the classical finite element method with linear shape functions. With $\beta = 0$ the tangent is computed using the projection part and leads to a rank deficient tangent. For the stabilization parameter in this work we choose $\beta^{stat} = 0.4$ and $\beta^{dyn} = 0$, which means that the stiffness matrix is stabilized by 40% of the FEM solution and the mass matrix is computed without any stabilization.

## 3 Numerical examples

### 3.1 Cook's membrane problem (2D)

The first example is the Cook's membrane problem in 2D. The geometrical setup and boundary conditions can be taken from 1(**a**). In this test a force driven scenario is modeled, where the force is applied at the right edge as a line load as depicted in Figure 1(**a**). The force is applied as half-sine with a maximum amplitude $P_{max} = 10000\ kN/mm$ at a time period of $T = 0.0005\ s$. The contour plots of the vertical displacement evolution for the deformation state $\{t = 0.00065\ s\}$ is sketched in Figure 1(**d**). Figure 3 shows a mesh refinement study with the element division of $2^N$ for N=2,4 from **a**-**b**. The solution converges for higher mesh resolution, as shown in Figure 3(**b**). A comparison with FEM underlines the accuracy of the results and emphasizes that the results are in a very good agreement.

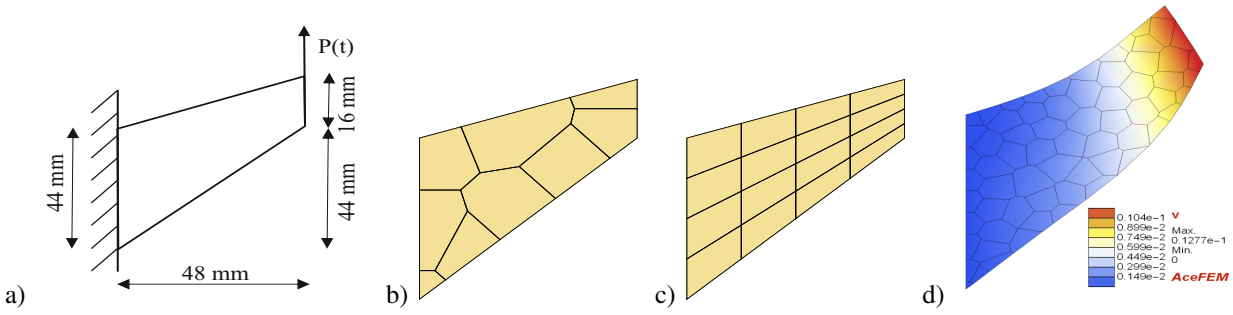


**Fig. 1:** 2D Cook's membrane. (**a**) Boundary Value Problem, (**b**) VEM Voronoi Mesh, (**c**) VEM Q2S Mesh, and (**d**) deformed Mesh.

### 3.2 Transversal vibration of a thick beam (3D)

In this test a 3D cantilever beam is investigated. The beam length, height and width is set to $\ell = 30\ mm$ and $h = b = 5\ mm$. Here a line load along the edge is applied at the end of the beam with $P_{max} = 6\ kN/mm$. The temporal course of the force is again given by a *half sine*. In this example we compare the virtual element H2S with the finite elements H2. The FEM H2 solution is computed with 3200 elements and can be seen as a *reference solution*. The virtual element VEM H2S is obtained with 256 elements. Figure 3**b** shows the maximum deformation state, representing the deflection $w$. Here the nonlinear behavior is clearly observed due to the dynamic effects at finite strains. Figure 3**a** illustrates the displacement over time response at the end of the beam at the center of the cross section. It is interesting to note that despite the use of linear ansatz functions VEM H2S produces nearly the same results as the reference solution. This is due to the fact that the stabilization uses the bending modes. In conclusion, the presented formulation depicts very good results also in the 3D case.

## 4 Summary and conclusion

In this work, we present an efficient low order virtual element formulation for nonlinear elastodynamics. The virtual element results show a very good match with finite element results. Arbitrary shaped elements with a various number of nodes could

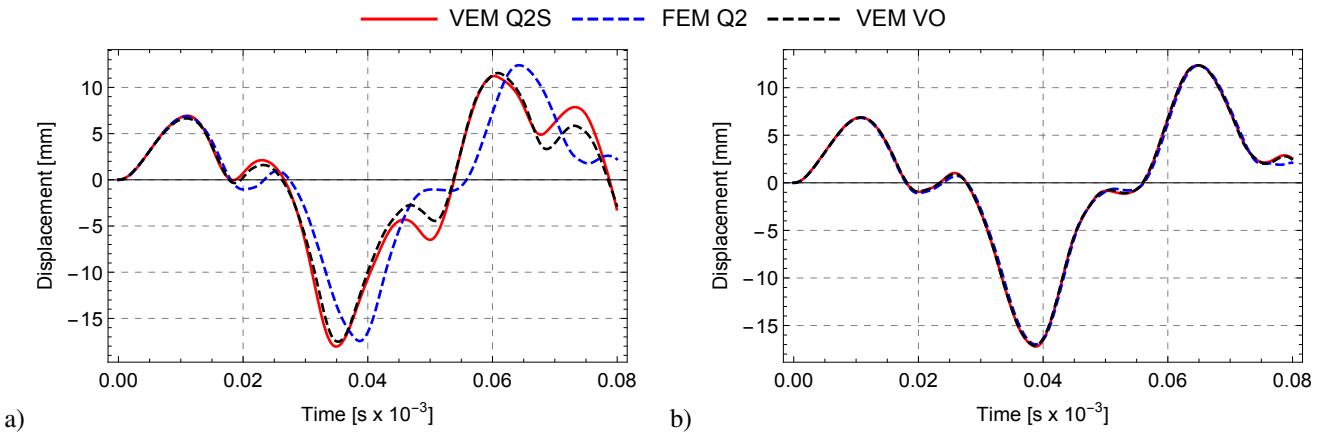


**Fig. 2:** 2D Cook's membrane. Convergence Study - Displacement over time response for different element divisions $2^N$, with $N = 2$ in (**a**) and $N = 4$ in (**b**).

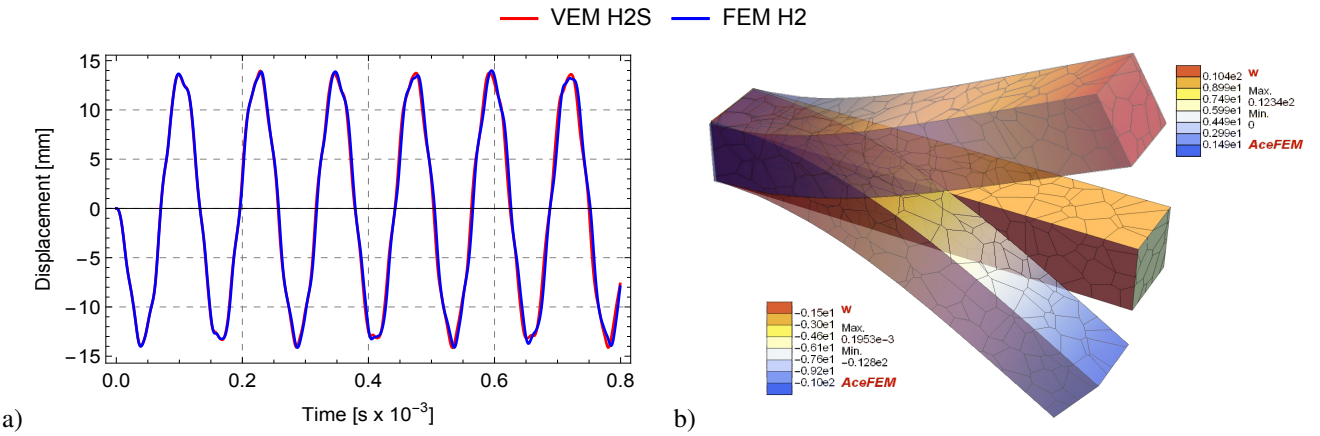


**Fig. 3:** 3D Example - (**a**) Displacement over time response and (**b**) undeformed and maximal deformed mesh.

be used successfully for the simulations. The computation of the mass-matrix was performed using the projection part and does not need any stabilization.

**Acknowledgements** The authors gratefully acknowledges support for this research by the "German Research Foundation" (DFG) in (i) the COLLABORATIVE RESEARCH CENTER **CRC 1153** and (ii) the PRIORITY PROGRAM **SPP 2020** within their *second funding phases*. Open access funding enabled and organized by Projekt DEAL.

## References

[1] B. Hudobivnik, F. Aldakheel, and P. Wriggers. A low order 3D virtual element formulation for finite elasto–plastic deformations. Computational Mechanics. 10.1007/s00466-018-1593-6, 2018.

[2] F. Aldakheel, B. Hudobivnik, and P. Wriggers. Virtual element formulation for phase-field modeling of ductile fracture. International Journal for Multiscale Computational Engineering, 17(2):181200, 2019.

[3] A. Hussein, F. Aldakheel, B. Hudobivnik, P. Wriggers, P-A. Guidault, and O. Allix. A Computational framework for brittle crack propagation based on an efficient virtual element method. Finite Elements in Analysis and Design, 159:1532, 2019.

[4] F. Aldakheel, B. Hudobivnik, and P. Wriggers. Virtual elements for finite thermo-plasticity problems. Computational Mechanics, 64:13471360, 2019.

[5] M. Cihan, F. Aldakheel, B. Hudobivnik, and P. Wriggers. Virtual element formulation for finite strain elastodynamics. arXiv preprint arXiv:2002.02680, 2020.

[6] F. Aldakheel, B. Hudobivnik, A. Hussein, and P. Wriggers. Phase-Field Modeling of Brittle Fracture Using an Efficient Virtual Element Scheme. Computer Methods in Applied Mechanics and Engineering. 341. 10.1016/j.cma.2018.07.008, 2018.

[7] P. Wriggers, B.D. Reddy, W. Rust, and B. Hudobivnik. Efficient virtual element formulations for compressible and incompressible finite deformations. Computational Mechanics, 60, 253-268, 2017.